

Preparation of nano-flower-like SnO₂ particles and their applications in efficient CdS quantum dots sensitized solar cells

Zhang Lan^{1,2,3} · Lu Liu^{1,2,3} · Miaoliang Huang^{1,2,3} · Jihuai Wu^{1,2,3} · Jianming Lin^{1,2,3}

Received: 26 April 2015 / Accepted: 30 June 2015 / Published online: 8 July 2015
© Springer Science+Business Media New York 2015

Abstract Two kinds of hierarchical SnO₂ particles as nano-flower-like SnO₂ particles (NF-SnO₂) and mesoporous-sphere-like SnO₂ particles (MS-SnO₂) have been synthesized and used in CdS quantum dots (QDs) sensitized solar cells (QDSSC). TEM images show that NF-SnO₂ particles compose well interconnected nanoplates and MS-SnO₂ spheres are consisted with large numbers of SnO₂ nanoparticles with size about 7 nm. Owing to the larger Brunauer–Emmett–Teller surface area of NF-SnO₂ particles, NF-SnO₂ photoelectrode can load higher amounts of CdS QDs and shows enhanced light absorbance, resulting in higher short-circuit current density compared with that of MS-SnO₂ photoelectrode. The electrochemical impedance spectroscopy analysis results show that the QDSSC with NF-SnO₂ photoelectrode has a higher charge recombination resistance and a longer electron lifetime, so its photovoltaic performance is better than that of the QDSSC with MS-SnO₂ photoelectrode. The QDSSC with NF-SnO₂ photoelectrode can attain 3 % power conversion efficiency, which is higher than that of the cell with MS-SnO₂ photoelectrode (1.97 %).

1 Introduction

Dye-sensitized solar cells (DSSCs) have been intensively studied as a new kind of low cost and efficient solar cells in the past decades [1]. A typical DSSC contains three main components: a mesoporous metal oxide film coated with a monolayer of a light harvesting dye, a counter electrode pasted with an electrochemical active catalyst, and an electrolyte containing a suitable kind of redox species or hole-transporter [2]. As a key component, the light harvesting dye influences the photovoltaic performance of DSSCs greatly. The current state of the art DSSCs are based upon organometallic dyes and organic dyes [3]. The power conversion efficiency (PCE) of the zinc porphyrin DSSCs with Cobalt (II/III)—based redox electrolyte has already exceeded 12 % at AM 1.5 G 100 mW cm⁻² [4]. More recently, there also has been extensive interest in utilizing semiconductor nanocrystals (or quantum dots, QDs) for harvesting light energy owing to some special characteristics of QDs such as multiple exciton generation, extremely high molar extinction coefficient, size-dependent bandgaps, and so on [5]. Some kinds of metal-chalcogenide-based QDs have already been used in quantum dot sensitized solar cells (QDSSCs), and the continuously increased PCE is obtained [6]. For example, the PCE of QDSSCs sensitized by CdSe_xTe_{1-x} QDs can exceed 6 % [7]; the PCE of QDSSCs sensitized by Mn-doped-CdS/CdSe QDs can attain to 5.42 % [8].

In DSSCs and QDSSCs, another component of mesoporous metal oxide film also plays important role in influencing the photovoltaic performance of the cells because it not only supplies large surface area to adsorb light harvesting dyes or QDs but also serves as a pathway for diffusing photo-injected electrons [9, 10]. Moreover, high light scattering ability of the film is also needed for

✉ Zhang Lan
308751201@qq.com; lanzhang@hqu.edu.cn

¹ Engineering Research Center of Environment-Friendly Functional Materials, Ministry of Education, Xiamen, China

² Key Laboratory of Functional Materials for Fujian Higher Education, Xiamen, China

³ Institute of Materials Physical Chemistry, Huaqiao University, Xiamen 361021, China

better harvesting light [11]. Till now, the most commonly used mesoporous metal oxide film is based on TiO₂ nanocrystalline particles. For enhancing light scattering, their hierarchical counterparts are also usually used [12]. Compared to TiO₂, SnO₂ has some advantages. Its electron-mobility (about 100–200 cm² V⁻¹ S⁻¹) is orders of magnitude higher than that of TiO₂ (about 0.1–1 cm² V⁻¹ S⁻¹), so its electron diffusion rate is much faster than that of TiO₂ [13]. The conduction band minimum (CBM) of SnO₂ is also more negative than that of TiO₂, so the potential difference between the LUMO of dyes or QDs and CBM of SnO₂ is larger, resulting in higher electron injection efficiency and extending the utilization of low band gap dyes or QDs [14]. Although the SnO₂ based DSSCs show much poorer performance compared with TiO₂ based DSSCs due to the serious dark recombination [15], the above mentioned advantages are quite desirable for high efficiency QDSSCs to achieve full wavelength response, fast electron transportation, and even separation of generated multiple excitons [16].

The PCE of pure CdS QDs sensitized nanocrystalline TiO₂ based QDSSCs seldom attains to 3 %, and the best value is only 2.53 % [8]. Owing to the above mentioned advantages of SnO₂ materials, we try to utilize nano-flower-like SnO₂ particles consisting well connected nanoplates (NF-SnO₂) to fabricate pure CdS QDs sensitized solar cells, which show a high PCE about 3 %. For comparison, mesoporous-sphere-like SnO₂ particles (MS-SnO₂) are also synthesized and used in the photoelectrodes of QDSSCs. The PCE, UV–Vis absorption and diffusion spectra, and electrochemical impedance spectroscopy (EIS) have been measured in order to scrutinize charge generation, transportation, and recombination in the two kinds of SnO₂ particles based QDSSCs. It is found that QDSSCs with NF-SnO₂ particles show obviously enhanced photovoltaic performance compared with that of the cells with MS-SnO₂ particles.

2 Experimental section

2.1 Materials

All reagents including stannic sulfate (SnSO₄), acid trisodium citrate (Na₃C₅H₆O₇·2H₂O), cadmium nitrate tetrahydrate [Cd(NO₃)₂·4H₂O], sodium sulfide tetrahydrate (Na₂S·4H₂O), and zinc acetate dehydrate [Zn(CH₃COO)₂·2H₂O] were AR Grade, purchased from aladdin Chemical Reagent Co., Ltd, and used without further treatment. Conducting glass plates (FTO glass, Fluorine doped tin oxide over-layer, sheet resistance 15 Ω square⁻¹, purchased from Nippon Sheet Glass. JP) were used as substrates for precipitating SnO₂ films.

2.2 Preparation of SnO₂ micro-spheres and flower-like particles based photoelectrodes

The MS-SnO₂ spheres were prepared from the hydrolysis reaction of tin sulfate. In a typical procedure, 0.4 g SnSO₄ was dissolved in 60 ml mixture solution containing 15 ml water and 45 ml ethanol. Then the solution was stirred vigorously for 30 min to get a white suspension. The product was collected by centrifugation after washed with distilled water several times. Then the product was dried at 80 °C and calcinated at 500 °C for 2.5 h in air [17].

The NF-SnO₂ particles were prepared from the hydrolysis reaction of tin sulfate combining with hydrothermal treatment. In a typical experiment, 1 g (5 mmol) SnSO₄ and 4.4 g (15 mmol) Na₃C₅H₆O₇·2H₂O were dissolved in a mixture of ethanol (10 ml) and deionized water (90 ml) with vigorous stirring for 1 h to form a homogeneous solution. Subsequently, the mixture was transferred into a Teflon-lined stainless steel autoclave and kept at 160 °C for 24 h. After hydrothermal procedure, the autoclave was cooled down to room temperature. The precipitates were collected by centrifugation, washed several times with deionized water and ethanol, respectively, and dried at 80 °C for 12 h. Finally, the NF-SnO₂ particles were obtained by annealing the precipitates at 500 °C for 2.5 h in air [18].

2.3 Preparation of CdS sensitized SnO₂ micro-spheres and flower-like particles based photoelectrodes

To prepare SnO₂ paste, 0.2 g ethylene cellulose was added to 5 g terpeneol solvent. Then 0.2 g MS-SnO₂ spheres or NF-SnO₂ particles were added to 10 ml absolute ethanol. Finally, the above two solutions were mixed and stirred several hours to yield a slurry. The slurry was spread uniformly onto a FTO glass substrate. After drying in air, the film was sintered at 500 °C for 30 min. TiCl₄ post-treatment was performed by dipping the SnO₂ films into 0.5 M TiCl₄ aqueous solution for 30 min at 80 °C, then washing the electrodes with distilled water to remove residual TiCl₄, and finally sintering again at 500 °C in air for 30 min.

CdS QDs were deposited on the electrodes using successive ionic layer adsorption and reaction method (SILAR). The SnO₂ films on FTO glasses were dipped in a solution containing 0.1 M Cd(NO₃)₂·4H₂O in ethanol for 5 min and rinsed with ethanol. Subsequently, the electrodes were dipped in a methyl alcohol solution containing 0.1 M Na₂S·4H₂O for 5 min and washed with methanol. So the one cycle of deposition was finished. The same procedures were repeated five cycles to obtain suitable loading amount of CdS on the electrodes. After drying in air for a

few minutes, a ZnS protected layer was deposited onto the former prepared CdS sensitized SnO₂ photoelectrodes with 0.1 M Zn(CH₃COO)₂·2H₂O and 0.1 M Na₂S·9H₂O aqueous solutions by the same method. The deposition was done two cycles. The obtained samples were dried in air to finish the preparation processes of CdS sensitized SnO₂ photoelectrodes.

2.4 Assembling of CdS quantum dot sensitized solar cells

A Cu₂S counter electrode, which was formed in situ by soaking a magnetron sputtering Cu film on a FTO glass in a liquid electrolyte the same as that used in assembling cells, a prepared photoelectrode, and a drop of the liquid electrolyte containing 0.5 M Na₂S, 2 M S, and 0.2 M KCl in a methanol/water (7:3 by volume) solution were sandwiched together to form the cell [19].

2.5 Measurements

The morphologies of SnO₂ photoelectrodes were observed by a field emission scanning electron microscopy (FESEM) (S-4800, HITACHI) and a field emission transmission electron microscopy (FETEM) (JEM-2100). X-ray Diffraction (XRD) measurements were carried out with a Bruker D8, using Cu KR1 radiation (λ) 0.154059 nm). UV–Vis absorption spectra were measured with a UV–Vis 3100 spectrophotometer (Shimadzu, Japan). Electrochemical impedance spectroscopy (EIS) measurements were recorded using a CHI 660 C electrochemical workstation. The impedance spectra were analyzed with the Zview software. Photovoltaic tests were carried out by measuring the I–V characteristic curves under simulated AM 1.5 G solar illumination at 100 mW cm⁻² from a xenon arc lamp (CHF-XM500, Trusttech Co., Ltd, China) in air and recorded with a CHI 660 C electrochemical workstation. All samples were measured five times and the average data were taken.

3 Results and discussion

The typical XRD pattern of MS-SnO₂ spheres and NF-SnO₂ particles are shown in Fig. 1. The diffraction pattern of NF-SnO₂ particles is well matched with MS-SnO₂ spheres and all of the diffraction peaks are indexed to the rutile structure (JCPDS card no. 41-1445). The high intensity of diffraction peaks verifies the high crystallinity of NF-SnO₂ particles. No other impurity peaks are observed, which demonstrates the formation of high purity rutile phase.

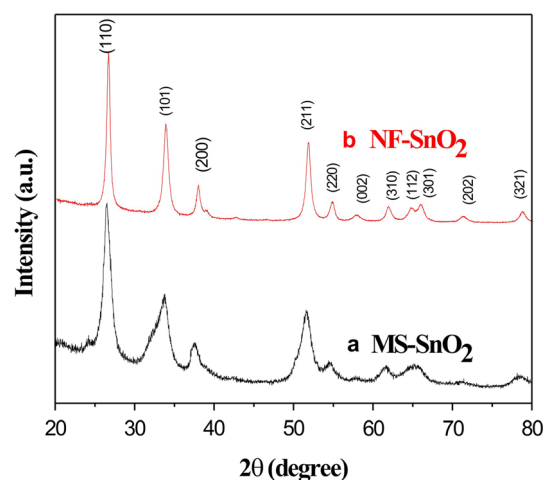


Fig. 1 XRD patterns of MS-SnO₂ spheres and NF-SnO₂ particles after annealed at 500 °C for 2.5 h

Figure 2 shows SEM, TEM and HRTEM images of MS-SnO₂ spheres (a, b, e) and NF-SnO₂ particles (c, d, f) after annealed at 500 °C for 2 h. From Fig. 2a, b, it can be seen that MS-SnO₂ spheres exhibit mesoporous structure with rough surface composing large numbers of SnO₂ nanoparticles with size about 7 nm. The diameter of MS-SnO₂ spheres is about 500 nm. As shown in Fig. 2c, d, NF-SnO₂ particles exhibit different morphology compared with that of MS-SnO₂ spheres. They look like nano-flowers consisting many pieces of nanoplates with average thickness about 8 nm. High resolution TEM (HRTEM) and selective area electron diffraction (SAED) were done to further investigate the structures of these particles as shown in Fig. 2e, f. The HRTEM images further confirm the observed morphologies. The lattice fringe spaces match the values of (110), (101) and (211) planes of rutile SnO₂ [20]. The diffraction rings of the SAED patterns for the samples (inset of Fig. 2e, f) reveal the polycrystalline nature of these particles. The diffraction rings can be indexed to (110), (101) and (211) planes, respectively. Moreover, one can find that the diffraction rings of the SAED pattern for NF-SnO₂ particles appear some discrete spots and are obviously clearer than that of MS-SnO₂ spheres, indicating higher crystallinity of NF-SnO₂ particles than the latter ones. So the obtained structural results from HRTEM and SAED are in good agreement with the XRD patterns shown in Fig. 1.

Figure 3 shows HRTEM and EDX spectrum of CdS QDs sensitized SnO₂ photoelectrodes. It is observed that the size of CdS QDs is smaller than 10 nm. The lattice fringe space value of 0.29 nm corresponds to (200) plane of the cubic phase of CdS (JCPDS card no. 80-0019) [21]. Meanwhile, EDX spectrum shows Sn, O, Cd and S peaks, respectively, resulting from SnO₂ and CdS. These results

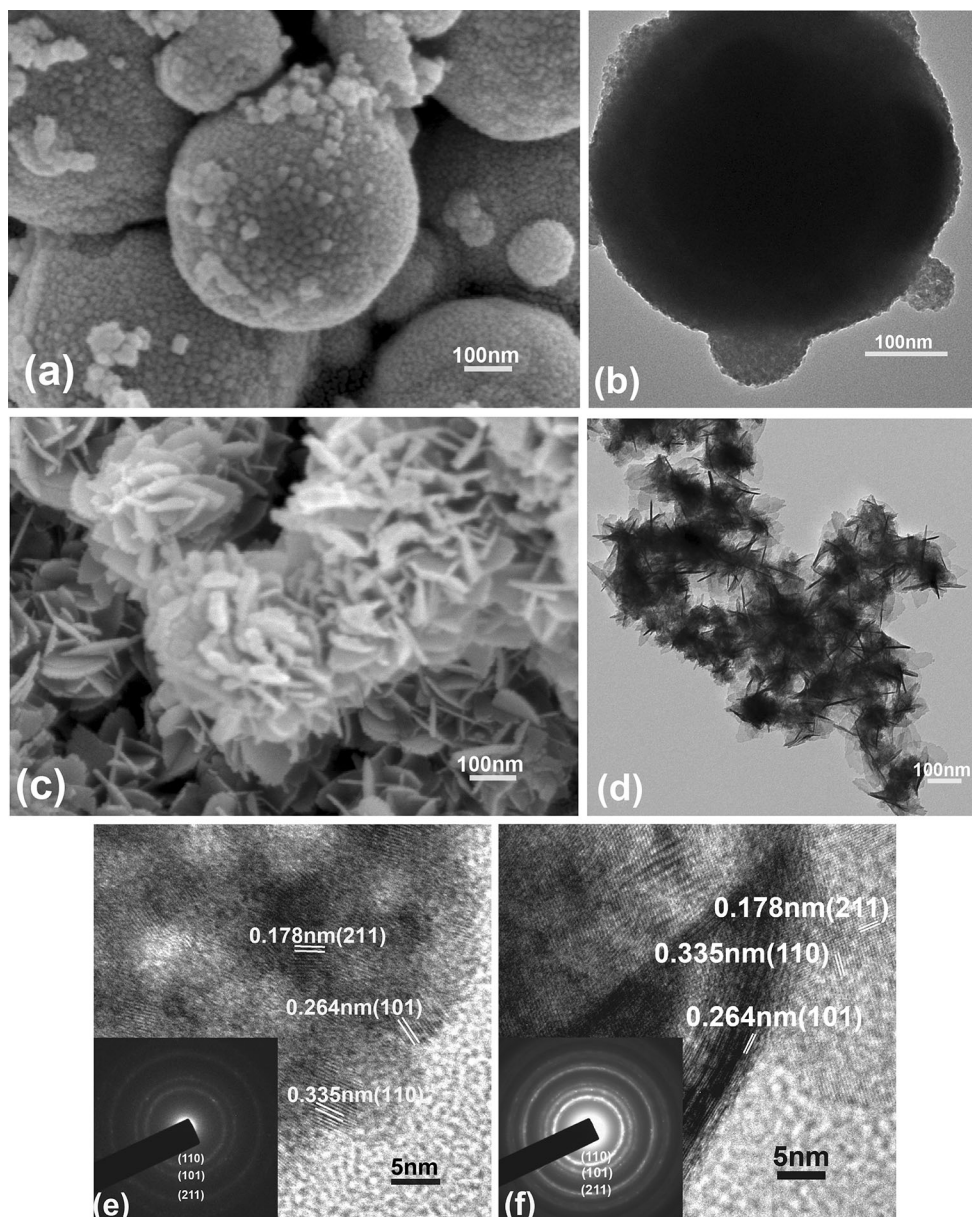


Fig. 2 SEM, TEM and HRTEM images of MS-SnO₂ spheres (a, b, e) and NF-SnO₂ (c, d, f) particles after annealed at 500 °C for 2 h. Their SAED patterns are shown *inset* of e and f

prove that CdS QDs have been successfully deposited on the SnO₂ particles.

Furthermore, MS-SnO₂ spheres and NF-SnO₂ particles are further investigated by nitrogen adsorption and desorption isotherms at 77 K (Fig. 4). The specific surface areas are measured by the Brunauer Emmett Teller (BET) method. All of the two isotherms can be approximately classified as type IV isotherms with a type H3 hysteresis loop, indicating the presence of slit-like pores in the materials, which are formed by the aggregation of sheet- or plate-like structure. The highly mesoporous structures are suggested by the prominent hysteresis loops at the relative

pressure of 0.45–1.0. The BET surface areas of these two samples are found to be 48.75 m² g⁻¹ and 72.86 m² g⁻¹, respectively.

Figure 5 shows the UV–Vis absorption spectra of CdS QDs sensitized MS-SnO₂ and NF-SnO₂ photoelectrodes. It is seen that the two samples have similar light absorbing spectra. Furthermore, the CdS QDs sensitized NF-SnO₂ photoelectrode shows an obviously enhanced absorbance in the short-wavelength region (200–500 nm). The higher BET surface area of NF-SnO₂ particles is beneficial for loading larger amounts of CdS QDs than that of MS-SnO₂ spheres.

Fig. 3 HRTEM images of CdS QDs sensitized MS-SnO₂ spheres (a) and NF-SnO₂ particles, and EDX spectrum of CdS QDs sensitized MS-SnO₂ spheres (c)

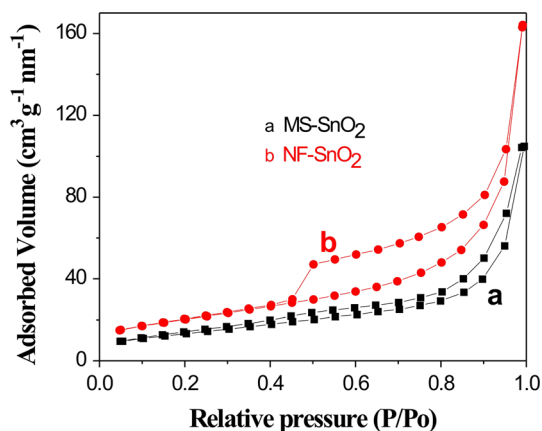
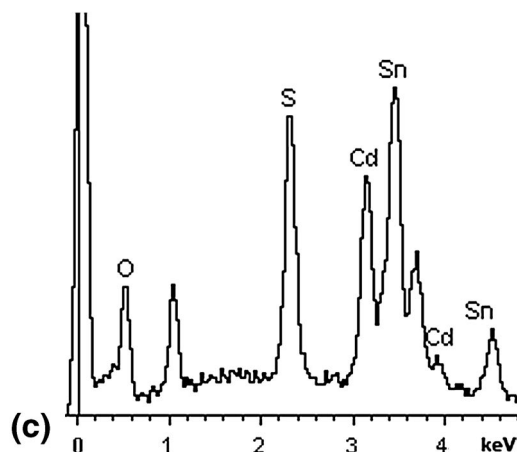
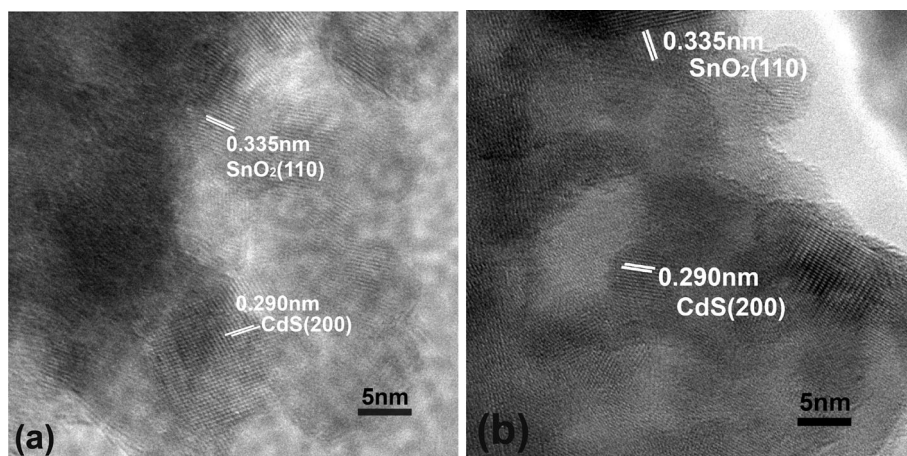


Fig. 4 N₂ adsorption–desorption isotherms of MS-SnO₂ spheres and NF-SnO₂ particles at 77 K

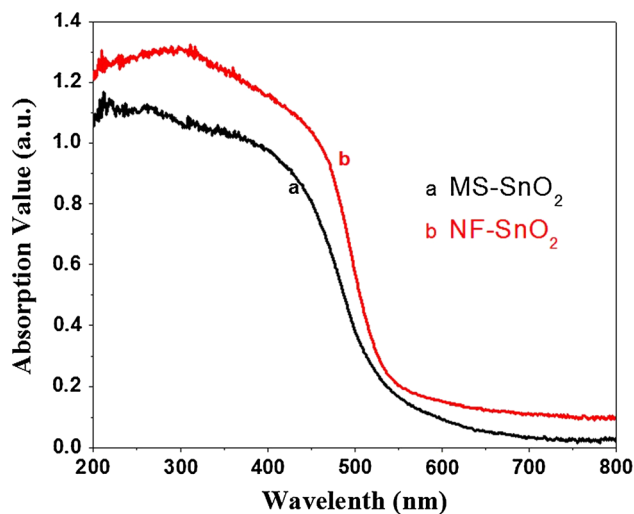


Fig. 5 UV–Vis absorption spectra of CdS QDs sensitized MS-SnO₂ and NF-SnO₂ photoelectrodes

Figure 6 shows photovoltaic performance of the QDSSCs. The related parameters such as short-circuit current density (J_{sc}), open-circuit voltage (V_{oc}), fill factor (FF), and power conversion efficiency (η) are listed in Table 1. It is seen that the QDSSC with CdS QDs sensitized NF-SnO₂ photoelectrode shows better photovoltaic

performance than that of the cell with MS-SnO₂ photoelectrode. This can be attributed to the following factors. The BET surface area of NF-SnO₂ particles is larger than

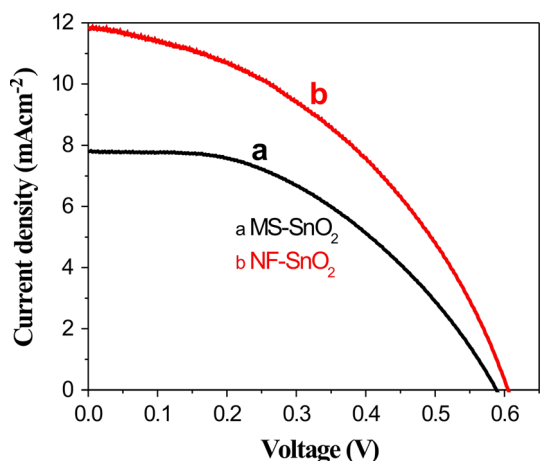


Fig. 6 I–V curves of CdS QDs sensitized MS-SnO₂ and NF-SnO₂ photoelectrodes based QDSSCs

that of MS-SnO₂ spheres, so the former ones can load larger amounts of CdS QDs. And NF-SnO₂ particles have bigger holes for deep diffusion of electrolyte into the QDSSC, which is also good for obtaining high photovoltaic performance.

EIS spectra of the QDSSCs with MS-SnO₂ and NF-SnO₂ photoelectrodes are measured and shown in Fig. 7. Under forward bias in the dark, electrons are transported through mesoporous SnO₂ film and react with electrolyte. At the same time, S is restored to S²⁻/S_x²⁻ at counter electrode. The dark reaction impedance due to electron

transfer from the conduction band of SnO₂ photoelectrodes to the electrolyte is presented by the semicircle in intermediate frequency region in the Nyquist plots. The bigger semicircle in the middle frequency region of Nyquist plots represents the slighter electron recombination at the CdS QDs sensitized SnO₂ photoelectrode/electrolyte interface [22]. In Fig. 7a, two semicircles can be recognized and fitted according to the equivalent circuit model shown inside the figure, the fitted data were listed in Table 2. The first semicircle (R_{ct1}) in high-frequency region (>10³ Hz) represents charge transfer at the counter electrode–electrolyte interface, while the second semicircle (R_{ct2}) in middle frequency (10–10² Hz) region reflects charge transfer at the photoelectrode electrolyte interface [23]. One can observe that the difference of R_{ct1} values of the two cells is similar, about 12–15 Ω cm². The R_{ct2} value of the NF-SnO₂ photoelectrodes is a bit higher than that of the MS-SnO₂ photoelectrode. Here, R_{ct2} is commonly thought to be determined by the charge recombination resistance, with partial contribution from transport resistance. The higher R_{ct2} of the NF-SnO₂ photoelectrode can be attributed to the higher charge recombination resistance compared with that of the cell with MS-SnO₂ photoelectrode in the dark.

In the bode-phase plots, two characteristic frequency peaks can be found. The electrons lifetime can be calculated from the middle frequency (f_{max}) as: τ = (1/2πf_{max}), where f_{max} is the peak frequency in the middle frequency range [24]. As listed in Table 2, the f_{max} value of QDSSC

Table 1 Photovoltaic parameters of QDSSCs presented in Fig. 6

Photoelectrode	V _{OC} (V)	J _{SC} (mA cm ⁻²)	FF	Eff (%)
MS-SnO ₂	0.589 ± 0.005	7.81 ± 0.12	0.429 ± 0.007	1.97 ± 0.08
NF-SnO ₂	0.609 ± 0.004	11.56 ± 0.09	0.426 ± 0.011	3.00 ± 0.12

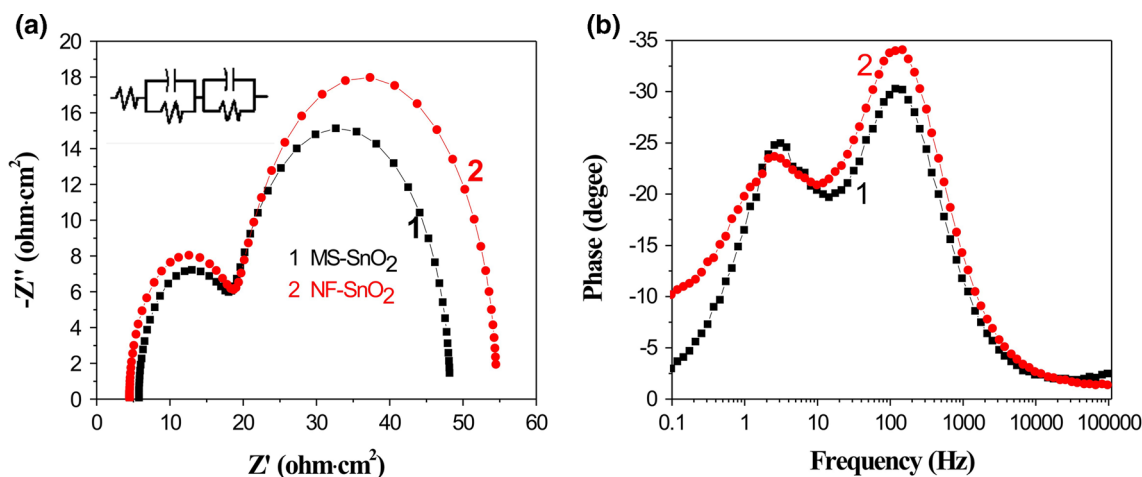


Fig. 7 EIS spectra of QDSSCs with CdS QDs sensitized MS-SnO₂ and NF-SnO₂ photoelectrodes. Nyquist plot (a), Bode plot (b)

Table 2 EIS parameters of QDSSCs with CdS QDs sensitized MS-SnO₂ and NF-SnO₂ photoelectrodes

Photoelectrode	R _{ct1} (Ω cm ²)	R _{ct2} (Ω cm ²)	f _{max} (Hz)
MS-SnO ₂	12.85 ± 0.07	29.63 ± 0.03	3.76 ± 0.04
NF-SnO ₂	14.67 ± 0.10	35.44 ± 0.08	2.55 ± 0.11

with NF-SnO₂ photoelectrode is 2.55 Hz, smaller than the value of MS-SnO₂ photoelectrode (3.76 Hz), resulting in a longer electron lifetime in QDSSC with NF-SnO₂ photoelectrode. An increased value of electron lifetime reveals the effective retardation of the charge recombination reaction between photo injected electrons with S²⁻/S_x²⁻ during the electron transport through the NF-SnO₂ photoelectrode compared with that of MS-SnO₂ photoelectrode. The results suggest that electrons can transport through the NF-SnO₂ photoelectrode with less diffusive hindrance and longer lifetime compared with that of MS-SnO₂ photoelectrode.

4 Conclusions

NF-SnO₂ particles have been successfully prepared by a simple hydrothermal method. When NF-SnO₂ particles are used in photoelectrode for QDSSC, they exhibit excellent optical and electrical properties, which are better than that of MS-SnO₂ spheres. Owing to larger BET surface area of NF-SnO₂ particles, NF-SnO₂ photoelectrode can load higher amounts of CdS QDs and shows enhanced light absorbance, which are beneficial for obtaining higher short-circuit current density compared with that of MS-SnO₂ photoelectrode. EIS analysis results show that the QDSSC with NF-SnO₂ photoelectrode has a higher charge recombination resistance and a longer electron lifetime, so its photovoltaic performance is better than that of the QDSSC with MS-SnO₂ photoelectrode.

Acknowledgments The authors would like to acknowledge the support of the National Natural Science Foundation of China (Nos. U1205112, 51002053, and 61474047), the Key Project of the Chinese Ministry of Education (212206), the Fujian Provincial Science Foundation for Distinguished Young Scholars (2015J06011), the

Programs for Prominent Young Talents and New Century Excellent Talents in Fujian Province University, and the Promotion Program for Yong and Middle-aged Teacher in Science and Technology Research of Huaqiao University (ZQN-YX102).

References

1. T. Kinoshita, J.T. Dy, S. Uchida, T. Kubo, H. Segawa, *Nat. Photonics* **7**, 535 (2013)
2. M. Gratzel, *J. Photochem. Photobio. A Chem* **164**, 3 (2004)
3. I. Chung, B.H. Lee, J.Q. He, R.P.H. Chang, M.G. Kanatzidis, *Nature* **485**, 486 (2012)
4. A. Yella, H.W. Lee, H.N. Tsao, C. Yi, A.K. Chandiran, M.K. Nazeeruddin, E.W.G. Diau, C.Y. Yeh, S.M. Zakeeruddin, M. Gratzel, *Science* **334**, 629 (2011)
5. I. Hod, V.G. Pedro, Z. Tachan, F.F. Santiago, I.M. Sero, J. Bisquert, A. Zaban, Dye versus quantum dots in sensitized solar cells: participation of quantum dot absorber in the recombination process. *J. Phys. Chem. Lett.* **2**, 3032 (2011)
6. X. Zhang, Z. Lan, J. Wu, J. Lin, L. Fan, *J. Mater. Sci. Mater. Electron.* **24**, 1970 (2013)
7. Z. Pan, K. Zhao, J. Wang, H. Zhang, Y. Feng, X. Zhong, *ACS Nano* **7**, 5215 (2013)
8. P.K. Santra, P.V. Kamat, *J. Am. Chem. Soc.* **134**, 2508 (2012)
9. Z. Lan, J. Wu, J. Lin, M. Huang, *Electrochim. acta* **56**, 9926 (2011)
10. H. Chen, L. Zhu, Q. Hou, W. Liang, H. Liu, W. Li, *J. Mater. Chem.* **22**, 23344 (2012)
11. Z. Lan, J. Wu, J. Lin, M. Huang, *Funct. Mater. Lett.* **6**, 13500141 (2013)
12. L. Feng, J. Jia, Y. Fang, X. Zhou, Y. Lin, *Electrochim. Acta* **87**, 629 (2013)
13. S. Gubbala, V. Chakrapani, V. Kumar, M.K. Sunkara, *Adv. Funct. Mater.* **18**, 2411 (2008)
14. H.J. Snaith, C. Ducati, *Nano Lett.* **10**, 1259 (2010)
15. A.N.M. Green, E. Palomares, S.A. Haque, J.M. Kroon, J.R. Durrant, *J. Phys. Chem. B* **109**, 12525 (2005)
16. M.A. Hossain, J.R. Jennings, Z.Y. Koh, Q. Wang, *ACS Nano* **5**, 3172 (2011)
17. X. Yin, L. Chen, C. Li, Q. Hao, S. Liu, Q. Li, E. Zhang, T. Wang, *Electrochim. Acta* **56**, 2358 (2011)
18. M.A. Hossain, Z.Y. Koh, Q. Wang, *Phys. Chem. Chem. Phys.* **14**, 7367 (2012)
19. Y.L. Lee, C.H. Chang, *J. Power Sources* **185**, 584 (2008)
20. B. Cheng, J.M. Russell, W. Shi, L. Zhang, E.T. Samulski, *J. Am. Chem. Soc.* **126**, 5972 (2004)
21. X. Zhou, W. Fu, H. Yang, Y. Li, Y. Chen, M. Sun, J. Ma, L. Yang, B. Zhao, L. Tian, *Electrochim. Acta* **89**, 510 (2013)
22. X.Y. Yu, J.Y. Liao, K.Q. Qiu, D.B. Kuang, C.Y. Su, *ACS Nano* **5**, 9494 (2011)
23. G. Shang, J. Wu, S. Tang, L. Liu, X. Zhang, *J. Phys. Chem. C* **117**, 4345 (2013)
24. J. Bisquert, *J. Phys. Chem. B* **105**, 325 (2002)